

Raman scattering from spin fluctuations in $\text{Pr}_{2-x}\text{Ce}_x\text{CuO}_{4-y}$, $\text{Nd}_{2-x}\text{Ce}_x\text{CuO}_{4-y}$, and $\text{Sm}_{2-x}\text{Ce}_x\text{CuO}_{4-y}$

Izumi Tomeno, Masashi Yoshida, Kazuto Ikeda, Keishi Tai, Kenshi Takamuku, Naoki Koshizuka, and
 Shoji Tanaka

*Superconductivity Research Laboratory, International Superconductivity Technology Center,
 Shinonome, Koto-ku, Tokyo 135, Japan*

Kunihiko Oka and Hiromi Unoki

Electrotechnical Laboratory, Umezono, Tsukuba, Ibaraki 305, Japan

(Received 4 September 1990)

Antiferromagnetic excitations in single crystals of $\text{Pr}_{2-x}\text{Ce}_x\text{CuO}_{4-y}$, $\text{Nd}_{2-x}\text{Ce}_x\text{CuO}_{4-y}$, and $\text{Sm}_{2-x}\text{Ce}_x\text{CuO}_{4-y}$ were investigated as a function of Ce concentration using Raman scattering at room temperature. The introduction of electrons by Ce doping significantly broadens the two-magnon peak in the B_{1g} mode, indicating that zone-boundary magnons become damped with increasing Ce concentration. The existence of broad spin-pair-excitation spectra in the B_{1g} and B_{2g} modes at $x=0.15$ suggests that the short-range spin fluctuations persist in these electron-doped superconductors. The energy of the spin-pair-excitation peak in $\text{Pr}_{2-x}\text{Ce}_x\text{CuO}_{4-y}$ is not affected by doping up to $x=0.2$. This is similar in behavior to the $\text{Sm}_{2-x}\text{Ce}_x\text{CuO}_{4-y}$ system up to $x=0.17$. The absence of softening of the short-wavelength magnons in these systems is in marked contrast to the magnon softening behavior in $\text{La}_{2-x}\text{Sr}_x\text{CuO}_{4-y}$. The Raman spectra in $\text{Pr}_{2-x}\text{Ce}_x\text{CuO}_{4-y}$ make no distinction between the superconducting and the metallic regions. The highly damped magnetic-excitation spectra support the picture that the spin-spin correlation length in the present systems decreases gradually with increasing Ce concentration.

I. INTRODUCTION

The role of spin fluctuations in copper oxide superconductors has been extensively investigated because of the intimate connection between antiferromagnetism and superconductivity. Raman scattering experiments¹⁻⁶ have demonstrated the existence of two-dimensional (2D) zone-boundary spin-pair excitations within the CuO_2 planes of La_2CuO_4 and $\text{YBa}_2\text{Cu}_3\text{O}_6$. Magnon-pair scattering in parent crystals leads to the interpretation that the exchange constants J between nearest-neighbor Cu ions are much higher than the thermal energies kT_N , where T_N is the Néel temperature. As holes are introduced into the CuO_2 planes by adding oxygen or substituting Sr^{2+} for La^{3+} , two-magnon scattering peaks both broaden and shift to lower energies. In heavily doped $\text{La}_{2-x}\text{Sr}_x\text{CuO}_{4-y}$ and $\text{YBa}_2\text{Cu}_3\text{O}_{6+x}$, observations of energy-independent spectra indicate that spin fluctuations persist in the normal state of the superconductor where antiferromagnetic (AF) long-range order is destroyed.

The electron-doped superconductors $L_{2-x}\text{Ce}_x\text{CuO}_{4-y}$ ($L = \text{Pr}, \text{Nd}, \text{Sm}, \text{and Eu}$)⁷⁻⁹ have the T' tetragonal crystal structure, where the Cu atoms are square-planar coordinated by oxygens. In contrast to this, the Cu atoms in hole-doped $\text{La}_{2-x}\text{Sr}_x\text{CuO}_{4-y}$ are surrounded by oxygen octahedra. Raman scattering in Nd_2CuO_4 and Sm_2CuO_4 (Refs. 10 and 11) showed that two-magnon features are characterized by an exchange constant J of the order of 1000 cm^{-1} . According to neutron-diffraction stud-

ies,¹²⁻¹⁴ Nd_2CuO_4 and Pr_2CuO_4 are 2D spin- $\frac{1}{2}$ Heisenberg antiferromagnets with $T_N = 250-270 \text{ K}$. Destruction of AF long-range order by doping is common to the occurrence of superconductivity in all layered Cu-O-based materials. In addition, a reduction annealing is required to induce superconducting (SC) behavior in the $L_{2-x}\text{Ce}_x\text{CuO}_{4-y}$ system. In view of their suppression of the Néel state,^{15,16} both electron and hole doping are expected to have an influence on the interaction between nearest-neighbor Cu spins.

We carried out Raman scattering measurements on single crystals of $\text{Pr}_{2-x}\text{Ce}_x\text{CuO}_{4-y}$, $\text{Nd}_{2-x}\text{Ce}_x\text{CuO}_{4-y}$, and $\text{Sm}_{2-x}\text{Ce}_x\text{CuO}_{4-y}$ at room temperature, in the hope of deriving the spin fluctuations versus Ce concentration relationship. In particular, we examine the Raman spectra in $\text{Pr}_{2-x}\text{Ce}_x\text{CuO}_{4-y}$ in the range up to $x=0.2$ and $\text{Sm}_{2-x}\text{Ce}_x\text{CuO}_{4-y}$ up to $x=0.17$. We compare the present results with those for hole-doped $\text{La}_{2-x}\text{Sr}_x\text{CuO}_{4-y}$ and $\text{YBa}_2\text{Cu}_3\text{O}_{7-x}$ systems. The Ce concentration dependence of B_{1g} and B_{2g} spectra strongly suggests that short-range spin fluctuations remain in the electron-doped superconductors.

II. EXPERIMENTAL PROCEDURE

A. Crystal growth and characterization

We performed most of the Raman experiments using flux-grown single crystals. Platelike crystals of $\text{Pr}_{2-x}\text{Ce}_x\text{CuO}_{4-y}$, $\text{Nd}_{2-x}\text{Ce}_x\text{CuO}_{4-y}$, and

$\text{Sm}_{2-x}\text{Ce}_x\text{CuO}_4$ were grown from a CuO flux, using the phase diagram for the $\text{Nd}_2\text{O}_3\text{-CuO}$ system.^{17,18} Mixtures with concentration ratios for $[\text{L}_2\text{O}_3]:[\text{CeO}_2]:[\text{CuO}]$ of $(15-7.5x):7.5x:85$ (mole%) were heated in alumina crucibles up to 1300°C , held at this temperature for 2 h, cooled to 1000°C at a rate of 5°C/h , and then furnace cooled to room temperature. A number of crystals with large areas perpendicular to the c axis appeared on the surface of CuO flux. A typical crystal size was $3 \times 3 \times 0.1 \text{ mm}^3$. No polishing procedure was required, because the flux-grown crystals had shiny flux-free surfaces. Energy-dispersive x-ray analysis indicated that these crystals are free from the Al contamination which may originate from the alumina crucibles. Next, a cylindrical single crystal of $\text{Pr}_{1.85}\text{Ce}_{0.15}\text{CuO}_{4-y}$ was prepared using the traveling-solvent-floating-zone (TSFZ) method, as described in detail previously.¹⁷ In this case, we sliced the crystal perpendicular to the c axis and polished the cut surface. The $x = 0.15$ samples were annealed in an Ar atmosphere at 920°C for 48 h, and then quenched to room temperature.

The Ce content in each sample was determined by in-

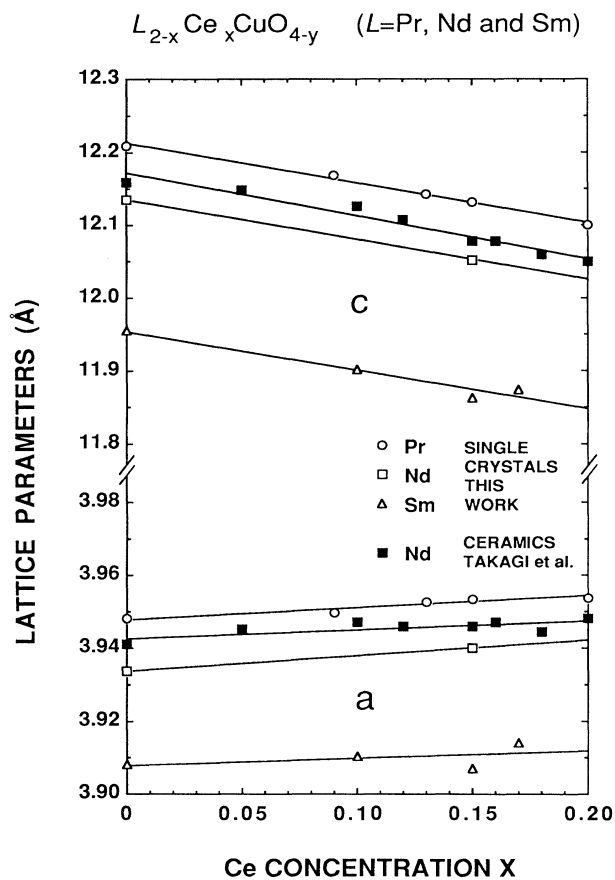


FIG. 1. Change in lattice parameters a and c with Ce concentration x for single crystals used for Raman experiments. The data for ceramic samples are taken from Takagi *et al.* (Ref. 8). Straight lines represent least-squares fits to the data.

ductively coupled-plasma (ICP) spectroscopy. The highest x values for Ce concentration in the flux-grown crystals are found to be 0.20 for the $\text{Pr}_{2-x}\text{Ce}_x\text{CuO}_{4-y}$ system and 0.17 for the $\text{Sm}_{2-x}\text{Ce}_x\text{CuO}_{4-y}$ system. The solubility limit of Ce may be different for the two systems. Electron-probe-microanalysis (EPMA) confirmed that the Ce is uniformly distributed. Room-temperature lattice parameters for the present samples were derived from a least-squares analysis of 25 x-ray reflections measured using a Rigaku AFC5R four-circle diffractometer. Figure 1 presents the change in the lattice parameters a and c with Ce concentration. These single-crystal results are consistent with the behavior in ceramic samples of

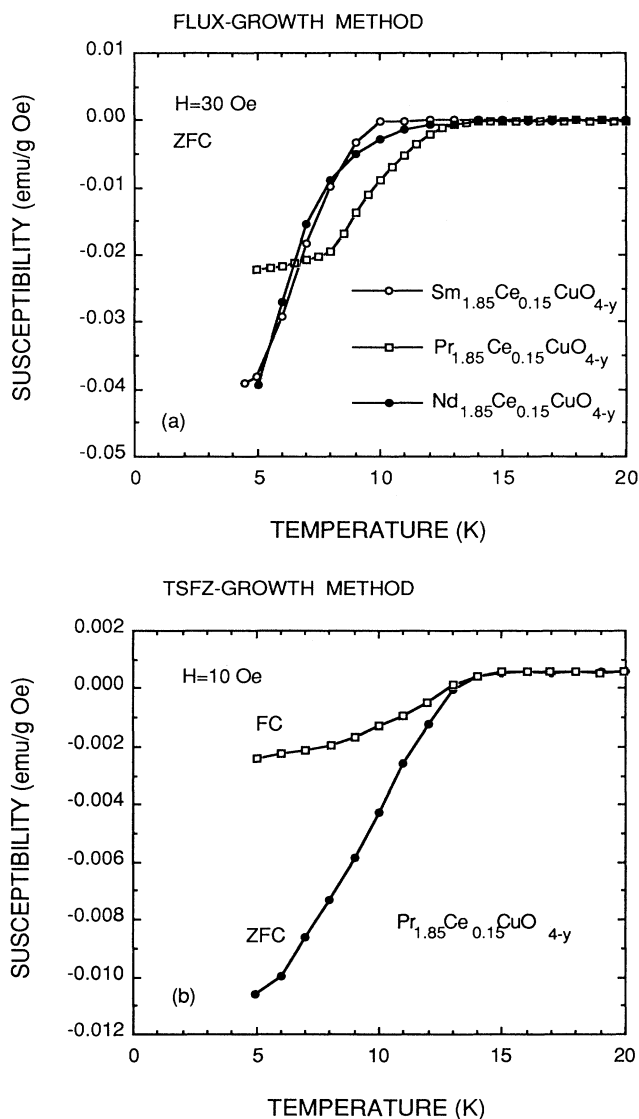


FIG. 2. Susceptibility χ for the crystals used in the Raman experiments. The data for flux-grown crystals in (a) are taken using the SQUID in the zero-field-cooled (ZFC) condition at a field of $H = 30 \text{ Oe}$. The curves in (b) represent both ZFC and field-cooled (FC) χ at 10 Oe in $\text{Pr}_{1.85}\text{Ce}_{0.15}\text{CuO}_{4-y}$ crystal grown with the TSFZ method.

$\text{Nd}_{2-x}\text{Ce}_x\text{CuO}_{4-y}$.⁸

Magnetization measurements were performed using a Quantum-Design superconducting-quantum-interference-device (SQUID) magnetometer. Figure 2 shows that the T_c values for the flux-grown crystals are 13 K for $\text{Pr}_{1.85}\text{Ce}_{0.15}\text{CuO}_{4-y}$, 11 K for $\text{Nd}_{1.85}\text{Ce}_{0.15}\text{CuO}_{4-y}$, and 10 K for $\text{Sm}_{1.85}\text{Ce}_{0.15}\text{CuO}_{4-y}$. The $\text{Pr}_{1.85}\text{Ce}_{0.15}\text{CuO}_{4-y}$ crystal grown with the TSFZ method exhibits a T_c of 14 K. These values were slightly lower than those for the ceramic samples with corresponding compositions reported by Tokura *et al.*⁷ We used these same samples for the Raman experiments.

B. Raman scattering

The Raman measurements were carried out in the backscattering configuration at room temperature. Linearly polarized light of 50 mW at 4880 Å from an argon-ion laser was focused on a spot of 0.1 mm diameter on the (001) plane. Scattered light was analyzed with a Jobin Yvon U1000 double-monochromator and detected using a Hamamatsu Photonics R943 photomultiplier. A half-wavelength plate was attached to the laser on condition of rotating the incident optical polarization, and a Polaroid polarizer was inserted at the entrance slit of the monochromator. All the spectra were calibrated to a standard lamp to correct for the response of the monochromator and detector. The polarization directions x and y refer to the tetragonal axes, and x' and y' are rotated on the z axis by 45° from the x and y axes in the (001)

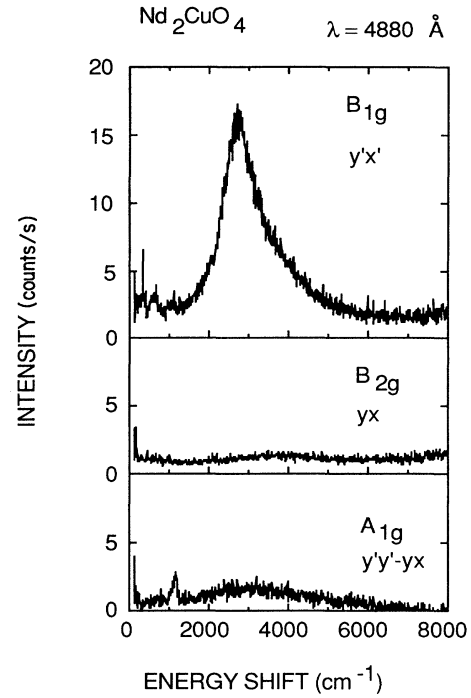


FIG. 4. Raman spectra of the Nd_2CuO_4 single crystal at room temperature.

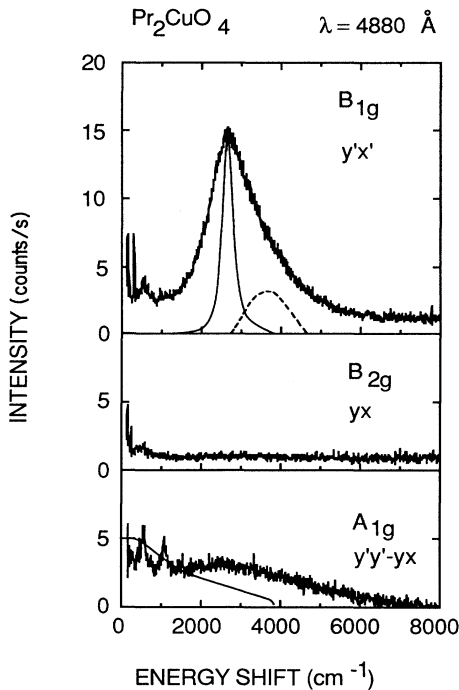


FIG. 3. Raman spectra of the Pr_2CuO_4 single crystal at room temperature. Solid lines represent the theoretical B_{1g} and A_{1g} line shapes based on the classical 2D Heisenberg model. Broken lines denote the deviation from the symmetric part in B_{1g} mode.

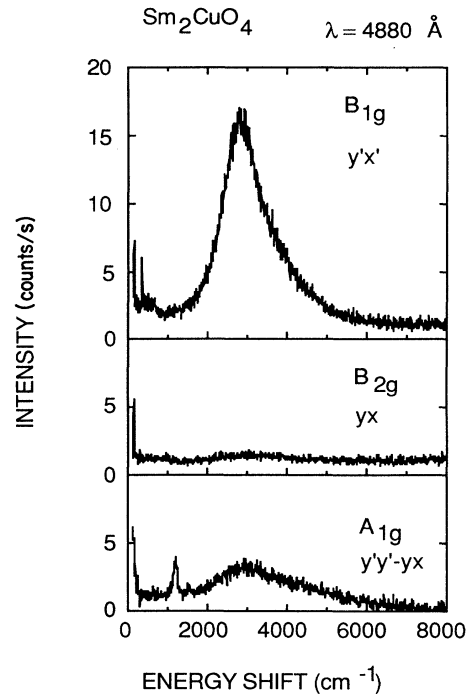


FIG. 5. Raman spectra of the Sm_2CuO_4 single crystal at room temperature.

plane. The geometries (y', x') and (y, x) yield the B_{1g} and B_{2g} Raman spectra, respectively.³ The configuration (y', y') gives rise to the sum of the A_{1g} and B_{2g} modes. Thus we determine the A_{1g} spectra by subtracting the (y', x') from the (y', y') signals. The A_{1g} spectra are therefore subject to the uncertainties of subtraction of two numbers of similar magnitude as well as the stray scattering.

III. RESULTS

Figures 3–5 show the B_{1g} , B_{2g} , and A_{1g} spectra up to 8000 cm^{-1} for the as-grown undoped crystals. The Ar annealing has practically no effect on the Raman spectra. Sharp structure below 1500 cm^{-1} in each mode is ascribed to phonon or two-phonon scattering. The simultaneous displacement of Cu and O atoms does not take place in these phonon modes.¹⁰ Here we will only treat the spectra due to magnetic scattering. The broad B_{1g} peak in Figs. 3–5 originates from two-magnon interactions. Characteristic features of the B_{1g} spectra are summarized in Table I. Several points are notable for the results on Pr_2CuO_4 , Nd_2CuO_4 , and Sm_2CuO_4 . (1) The energy $\hbar\omega_p$ for the peak-position is far larger than the thermal energy $kT_N = 190 \text{ cm}^{-1}$. (2) The energy $\hbar\omega_p$ increases with decreasing Cu-Cu distance a in the CuO_2 plane. (3) Each spectrum has an asymmetric line shape whose center of gravity $\hbar\omega_c$ is higher than the $\hbar\omega_p$ value. We calculate the $\hbar\omega_c$ value after the subtraction of phonon and background contributions, based on the assumption that the background scattering decreases linearly with increasing energy. (4) The A_{1g} spectrum in each parent crystal also has a peak at the same $\hbar\omega_p$ value, although its intensity is much lower than the B_{1g} peak intensity. (5) The B_{2g} mode has a weak, energy-independent intensity that is consistent with the selection rules for the undoped crystals.

The Ce concentration dependence of the Raman spectra is shown in Fig. 6 for $\text{Pr}_{2-x}\text{Ce}_x\text{CuO}_{4-y}$, and in Fig. 7 for $\text{Sm}_{2-x}\text{Ce}_x\text{CuO}_{4-y}$. Based on the phase diagram presented by Uchida *et al.*,¹⁵ the flux-grown crystals span the AF, SC, and metallic phases at 0 K; crystals up to $x = 0.13$ belong to the AF phase, the $x = 0.15$ and the $x = 0.17$ samples are the SC phase, and the $x = 0.2$ sample corresponds to the metallic phase. Doping in the AF

region suppresses the B_{1g} peak intensity and significantly broadens its linewidth. Figure 6(a) demonstrates this behavior for $\text{Pr}_{2-x}\text{Ce}_x\text{CuO}_{4-y}$ with $x = 0, 0.09$, and 0.13 . In $\text{Sm}_{1.9}\text{Ce}_{0.1}\text{CuO}_{4-y}$, the B_{1g} mode exhibits a 2400-cm^{-1} full width at half maximum (FWHM), double the value for $\text{Sm}_2\text{CuO}_{4-y}$, as listed in Table I. In $\text{Pr}_{2-x}\text{Ce}_x\text{CuO}_{4-y}$ and $\text{Sm}_{2-x}\text{Ce}_x\text{CuO}_{4-y}$, $\hbar\omega_p$ values for the B_{1g} peak position are nearly constant in the AF region where the T_N is sensitive to the Ce concentration. As illustrated in Figs. 6(b) and 7(b), the introduction of electrons induces B_{2g} intensity around $\hbar\omega_p$. The A_{1g} peak disappears at high Ce concentrations. The A_{1g} intensity in $\text{Sm}_{1.9}\text{Ce}_{0.1}\text{CuO}_{4-y}$ decreases slowly with increasing energy. This is similar in behavior to the A_{1g} spectra for the highly doped crystals of $\text{Pr}_{1.9}\text{Ce}_{0.1}\text{CuO}_{4-y}$ and $\text{Nd}_{1.5}\text{Ce}_{0.15}\text{CuO}_{4-y}$.

Magnetic scattering in crystals of SC and metallic concentration ranges is distributed over a wide energy scale, as shown in Figs. 8 and 9. It is clear that both the $x = 0.15$ and the $x = 0.2$ samples have extremely broad B_{1g} peaks related to magnetic fluctuations.

Figure 8 exhibits the Raman spectra of $\text{Pr}_{1.85}\text{Ce}_{0.15}\text{CuO}_{4-y}$ single crystals prepared with the flux and the TSFZ methods. There is little discrepancy in the features between the two crystals, indicating the intrinsic spectra in the normal state of the electron-doped superconductor. Note that both B_{1g} and B_{2g} spectra have broad peaks in the range between 2000 and 4000 cm^{-1} . As illustrated in Figs. 9 and 10, similar behavior is found for $\text{Nd}_{1.85}\text{Ce}_{0.15}\text{CuO}_{4-y}$ and for $\text{Sm}_{1.85}\text{Ce}_{0.15}\text{CuO}_{4-y}$.

IV. DISCUSSION

A. Undoped crystals

We begin by interpreting Raman features for $L_{2-x}\text{Ce}_x\text{CuO}_{4-y}$ ($L = \text{Pr}, \text{Nd}, \text{and Sm}$) in the AF region in terms of a spin-wave theory including magnon-magnon interactions. The Heisenberg Hamiltonian, which describes adequately the AF nature of undoped crystals, is given by

$$H = J \sum_{\langle i, j \rangle} \mathbf{S}_i \cdot \mathbf{S}_j, \quad (1)$$

where the sum is over nearest-neighbor pairs $\langle i, j \rangle$ of

TABLE I. Raman scattering features and related physical parameters for crystals in the AF region. Energies $\hbar\omega_p$ and $\hbar\omega_c$ refer to the peak and the center of gravity for two-magnon B_{1g} spectra, respectively. Exchange constants J were obtained from the classical relation $\hbar\omega_p = 2.7J$.

	$\hbar\omega_p$ (cm^{-1})	$\hbar\omega_c$ (cm^{-1})	FWHM (cm^{-1})	J (cm^{-1})	T_N (K)	a (\AA)
Pr_2CuO_4	2650	2990	1550	980	255 ^a	3.948
$\text{Pr}_{1.91}\text{Ce}_{0.09}\text{CuO}_{4-y}$	2650	2940	2000	980	160 ^a	3.950
$\text{Pr}_{1.87}\text{Ce}_{0.13}\text{CuO}_{4-y}$	2600	2880	2000	960	120 ^a	3.953
Nd_2CuO_4	2750	3000	1200	1020	255 ^b	3.934
Sm_2CuO_4	2800	3020	1200	1040		3.909
$\text{Sm}_{1.9}\text{Ce}_{0.1}\text{CuO}_{4-y}$	2800	2800	2400	1040		3.910

^aReference 21.

^bReference 13.

spins S_i, S_j . Here we neglect an anisotropy field which determines the spin directions. Based on Eq. (1), the magnon dispersion relation is expressed as

$$\hbar\omega = JSz \left[1 - \frac{1}{4}(\cos k_x a + \cos k_y a)^2 \right]^{0.5}, \quad (2)$$

where $z=4$ is the number of nearest-neighbor magnetic sites, \mathbf{k} is the magnon wave vector. In the D_{2h} symmetry appropriate here, the Raman-scattering Hamiltonians H_R for the B_{1g} mode and H_R' for the A_{1g} mode are expressed as^{19,20}

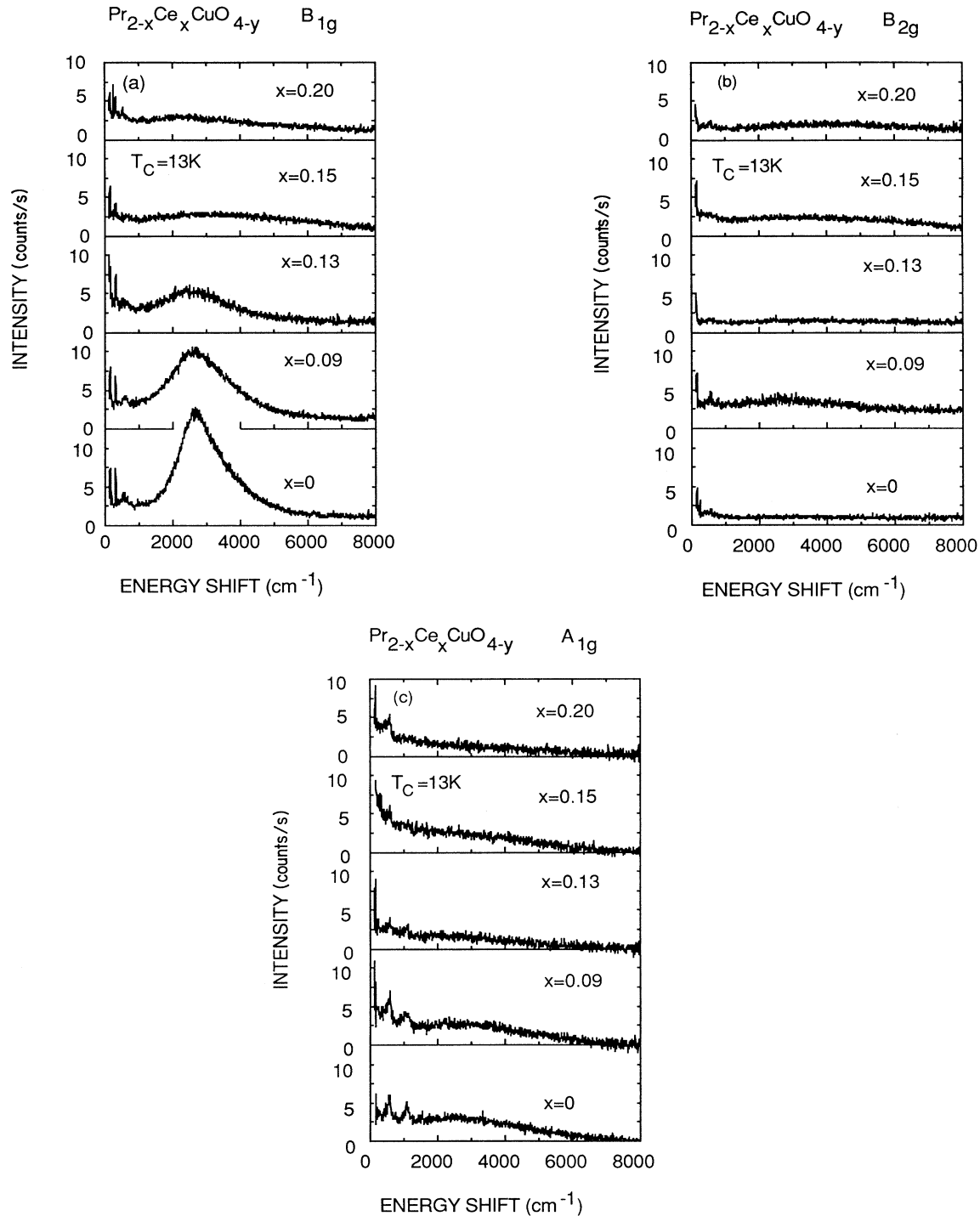


FIG. 6. Concentration dependence of Raman spectra for (a) B_{1g} , (b) B_{2g} , and (c) A_{1g} modes in $\text{Pr}_{2-x}\text{Ce}_x\text{CuO}_{4-y}$ at room temperature. Crystals with $x=0, 0.09$, and $x=0.13$ belong to the AF phase at 0 K. The $x=0.15$ crystal exhibits superconductivity at 13 K, as shown in Fig. 1. The $x=0.2$ crystal belongs to the metallic phase. All the spectra are taken using the flux-grown crystals.

$$H_R = \sum_{\langle i,j \rangle} (\mathbf{E}_{\text{inc}} \cdot \boldsymbol{\sigma}_{ij})(\mathbf{E}_{\text{sc}} \cdot \boldsymbol{\sigma}_{ij}) \mathbf{S}_i \cdot \mathbf{S}_j, \quad (3)$$

$$H_{R'} = \sum_{\langle i,j \rangle} (\mathbf{E}_{\text{inc}} \cdot \mathbf{E}_{\text{sc}}) \mathbf{S}_i \cdot \mathbf{S}_j, \quad (4)$$

where E_{inc} and E_{sc} are the incident and scattered electric

fields and σ_{ij} is a unit vector connecting spin sites i and j . Zone-boundary magnon-pair excitations dominate the B_{1g} spectrum, while zone-center magnon-pairs participate in the A_{1g} spectrum. In the case of 2D square symmetry, Parkinson¹⁹ gave the Green's function for the B_{1g}

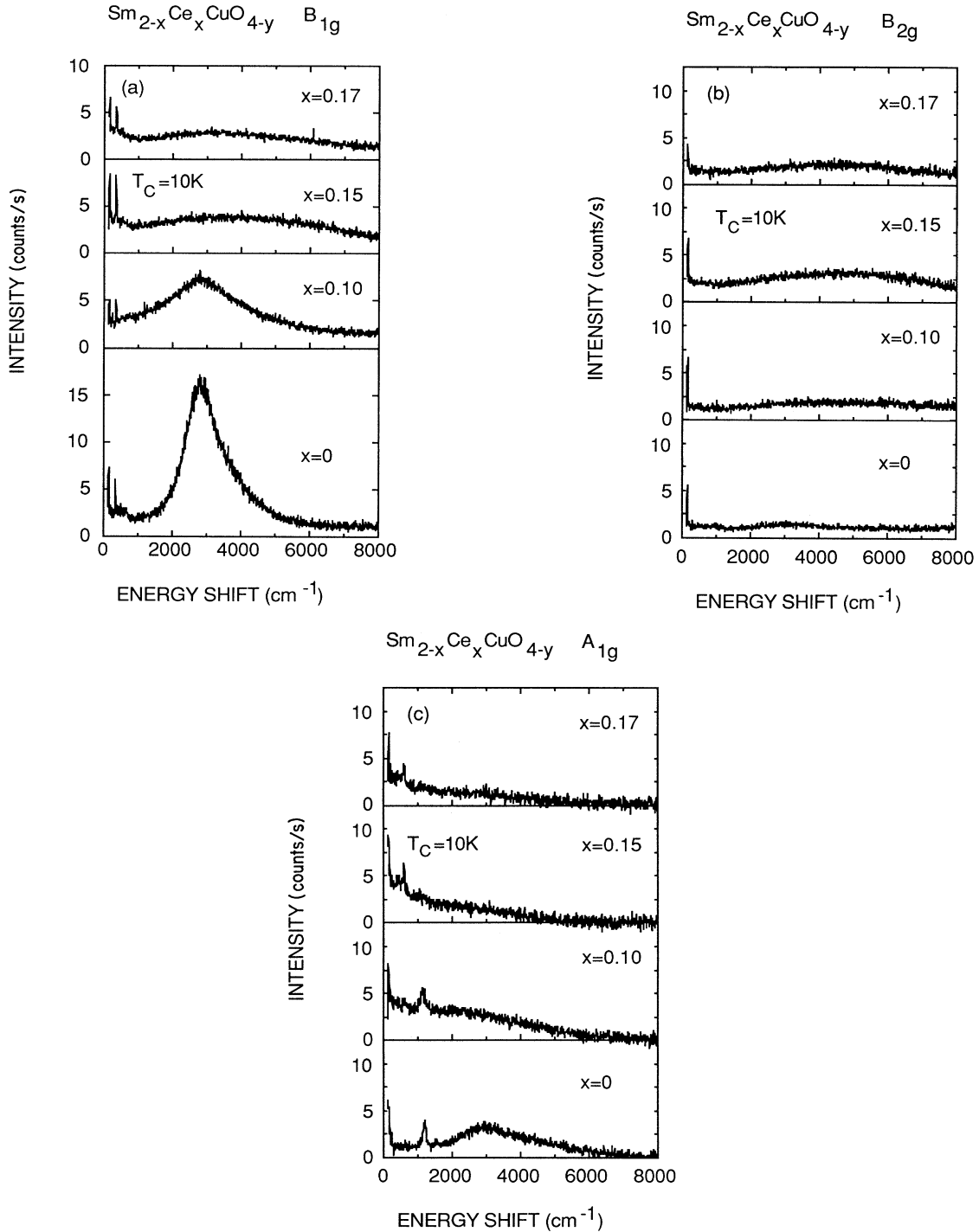


FIG. 7. Concentration dependence of Raman spectra for (a) B_{1g} , (b) B_{2g} , and (c) A_{1g} modes in $\text{Sm}_{2-x}\text{Ce}_x\text{CuO}_{4-y}$ at room temperature. The undoped and the $x = 0.10$ crystals belong to the AF phase at 0 K. The $x = 0.15$ and $x = 0.17$ crystals are superconductors.

mode, by taking into account the magnon-magnon interaction. The A_{1g} mode is Raman inactive, based on two-magnon interactions in a pure 2D square Heisenberg system. In the 3D case, Elliott and Thorpe²⁰ presented the Green's function for the A_{1g} mode which becomes

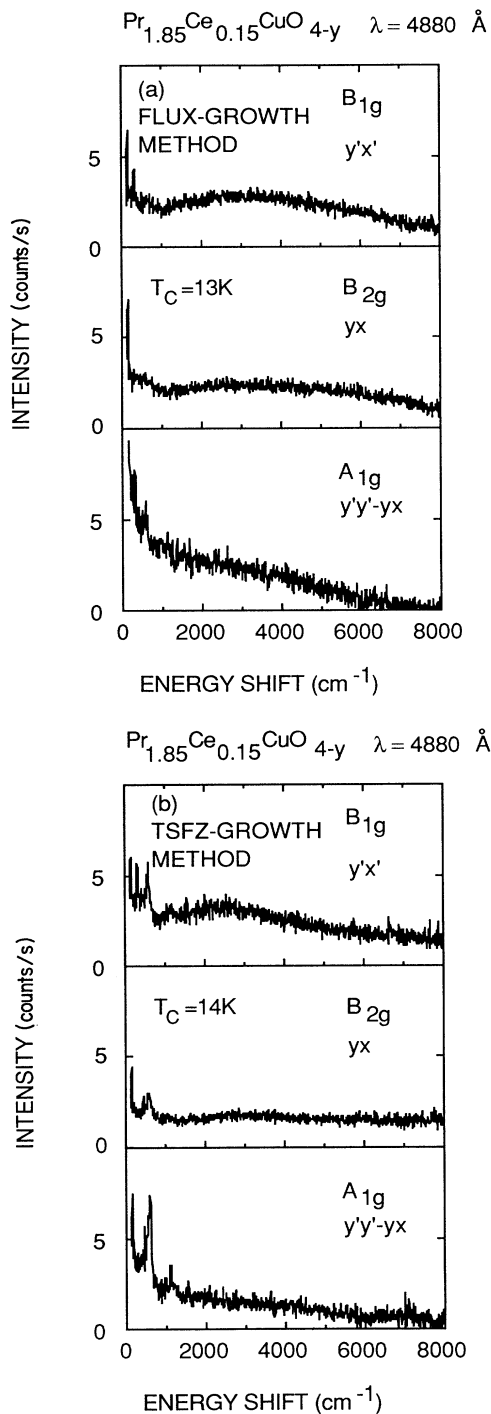


FIG. 8. Raman spectra of $\text{Pr}_{1.85}\text{Ce}_{0.15}\text{CuO}_{4-y}$ single crystals at room temperature. Data in (a) are obtained using the crystal grown with the flux method, and data in (b) are obtained using the crystal grown with the TSFZ method.

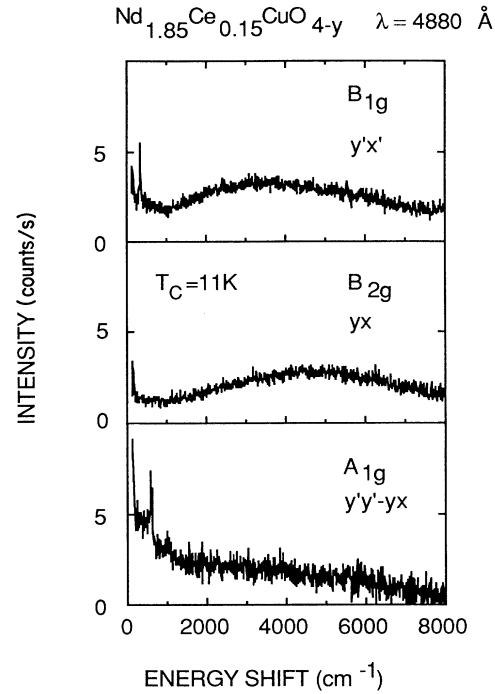


FIG. 9. Raman spectra of $\text{Nd}_{1.85}\text{Ce}_{0.15}\text{CuO}_{4-y}$ single crystals at room temperature.

Raman active in the presence of interactions higher than nearest-neighbor coupling. We transform the A_{1g} Green's function for the 3D symmetry into that for the 2D situation.

In Fig. 3 the observed line shapes for B_{1g} and A_{1g}

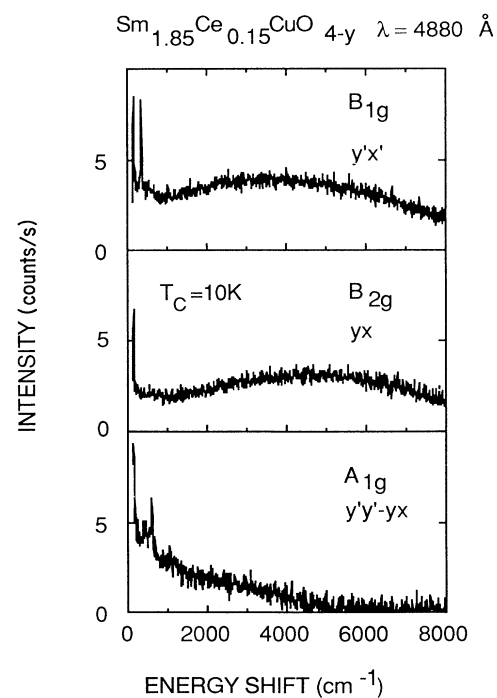


FIG. 10. Raman spectra of $\text{Sm}_{1.85}\text{Ce}_{0.15}\text{CuO}_{4-y}$ single crystals at room temperature.

modes in $\text{Pr}_2\text{CuO}_{4-y}$ are compared with the theoretical curves obtained from the imaginary part of the Green's function. According to this calculation, the B_{1g} spectrum exhibits a peak at $\hbar\omega_p = 2.7J$, while the A_{1g} intensity decreases gradually with increasing energy. The calculated B_{1g} curve is normalized by setting its maximum value equal to the observed peak, and the A_{1g} curve is plotted using the same normalizing parameters. Table I presents J values obtained from the relation $\hbar\omega_p = 2.7J$. Based on Eq. (2), the density of magnon states becomes significantly large at the zone boundary and small at the zone center. Large difference in the density of states can explain the observation that the B_{1g} peak intensities are dominant over the broad A_{1g} intensities.

The present J values listed in Table I are consistent with the values deduced from the neutron scattering measurement.²¹ Furthermore, the large- J values derived from Raman experiments¹⁻⁶ in $\text{La}_2\text{CuO}_{4-y}$ and $\text{YBa}_2\text{Cu}_3\text{O}_{6+x}$, are consistent with zone-center magnon dispersion relations determined by inelastic neutron diffraction.²²⁻²⁸ Consequently, the magnon-magnon interaction can account for the essential features of the peak in the B_{1g} mode. The mixture of Cu $3d_{x^2-y^2}$ and O $2p\sigma$ orbitals is responsible for the large- J value, based on the three-band Hubbard model. The exchange constant J in Eq. (1) is expressed as²⁹

$$J = \frac{4t_0^4}{\varepsilon_p^2 U} + \frac{4t_0^4}{2\varepsilon_p^3}, \quad (5)$$

where t_0 is the Cu-O hybridization matrix element, ε_p is the energy difference between Cu and O, and U is the on-site Coulomb repulsion at a Cu site. As listed in Table I, the J value derived from the B_{1g} peak-position for each $L_2\text{CuO}_{4-y}$ increases slightly with decreasing Cu-Cu distance a . Equation (5) predicts the J versus a relationship, on the assumption that t_0 is enhanced by the decrease in a and that ε_p and U are nearly independent of a .

It has been pointed out that the conventional spin-wave theory with $S = \frac{1}{2}$ cannot account for the broad B_{1g} line shape of layered Cu-O-based insulating materials.^{1-6,30} Figure 3 demonstrates that the observed B_{1g} spectrum in $\text{Pr}_2\text{CuO}_{4-y}$ extends to an energy higher than the two-magnon cut-off $4J = 3920 \text{ cm}^{-1}$, and that its linewidth (FWHM) is much broader than the prediction. In contrast to the 2D spin- $\frac{1}{2}$ case, the Green's function for the 2D spin-1 system gives an excellent fit to the two-magnon line shape for K_2NiF_4 using $J = 77 \text{ cm}^{-1}$ (Ref. 31). We discuss the following three possibilities in order to understand the extremely broad B_{1g} line shape in undoped Cu-O-based crystals.

One possible explanation is that a magnon damping gives rise to the broadening of the B_{1g} spectrum. According to Weber and Ford,³⁰ the Green's function including the magnon-damping term relaxes restrictions regarding the classical cut-off $4J$. They suggest that magnon damping in undoped Cu-O-based materials is due to the coupling to the continuum of electronic excitations related to the free carriers. In the undoped Cu-O crystals, the oxygen deficiencies may depend on the crystal-

growth condition. The Ar annealing process, however, exerts little influence on the two-magnon line shape in $L_2\text{CuO}_{4-y}$. In view of these results, the broadening of the spectrum is not caused by the oxygen deficiencies, but the intrinsic behavior of the parent crystals. In $L_2\text{CuO}_{4-y}$, magnons with the energy of 0.12 eV cannot couple directly with charge-transfer (CT) excitations whose energy is 1.5 eV.^{32,33} Tokura *et al.*³³ reported that the two-magnon line shapes in the Cu-O-based crystals are independent of their CT gaps. We expect that the energies of the zone-boundary magnons are considerably higher than those of the phonons. Thus it appears difficult to determine the common origin of magnon damping in all the Cu-O-based host crystals. The phenomenological treatment,³⁰ however, seems to be useful in understanding the linewidth broadening by Ce doping, as will be discussed later.

Another possibility is that quantum spin fluctuation effects contribute to the deviation from the calculated B_{1g} curve. The Heisenberg Hamiltonian in Eq. (1) can be expressed as

$$H = J \sum_{\langle i,j \rangle} S_i^z S_j^z + \frac{1}{2} J \sum_{\langle i,j \rangle} (S_i^+ S_j^- + S_i^- S_j^+), \quad (6)$$

where the spin operators S_i^+ and S_i^- are defined as $S_i^+ = S_i^x + iS_i^y$ and $S_i^- = S_i^x - iS_i^y$. In the classical picture, the Cu spins can be arranged so that all nearest-neighbors have antiparallel alignment. Thus it follows that the diagonal-next-nearest-neighbor Cu sites must have parallel spins. The second term of Eq. (6), which includes quantum fluctuations, reduces the average spin value $\langle S_i^z \rangle$ to three-fifths of the classical value $S = \frac{1}{2}$. Based on the Ising series-expansion method, Singh *et al.*⁶ and Sulewski *et al.*¹¹ showed that quantum spin fluctuations contribute significantly to the broadening of the B_{1g} spectrum. Furthermore, the second term of Eq. (6) allows both B_{2g} and A_{1g} modes to become Raman active. The quantum fluctuation theory yields the relationships between J and the cumulants of the line shape for each symmetry. Their calculation predicts that the centers of gravity $\hbar\omega_c$ for B_{1g} and A_{1g} spectra are equal to $3.6J$ and that $\hbar\omega_c$ for the B_{2g} spectrum is $3.9J$. The relation $\hbar\omega_c = 3.6J$ for the B_{1g} mode renormalizes the exchange constant derived from the classical equation $\hbar\omega_p = 2.7J$ downward by 18%. The observed relation $\hbar\omega_c > \hbar\omega_p$ is compatible with the cumulants.

The oxygen-oxygen hybridization in the undoped crystals may induce an additional coupling between the diagonal-next-nearest-neighbor Cu ions. The Heisenberg Hamiltonian including the diagonal exchange constant J'' is given by³⁴⁻³⁶

$$H = J \sum_{\langle i,j \rangle} S_i \cdot S_j + J'' \sum_{\langle i,k \rangle} S_i \cdot S_k, \quad (7)$$

where the sums over $\langle i,j \rangle$ and $\langle i,k \rangle$ denote all pairs of nearest-neighbor and diagonal-next-nearest-neighbor sites, respectively. The second term in Eq. (7) also renormalizes the magnon velocity at $k=0$ (Refs. 34 and 35), indicating the modification of the density of states. In $L_2\text{CuO}_{4-y}$, J'' is expected to be considerably smaller than J . The classical theory predicts that the small

exchange-constant J'' only contributes to the lower-energy part of the two-magnon spectra in the B_{1g} mode, on the assumption that the second term is superposed by the first term. This prediction seems inconsistent with the prediction for Eq. (6), although Eqs. (6) and (7) include the next-nearest-neighbor interaction. If we include a quantum fluctuation effect, Eq. (7) may yield realistic results. Unfortunately, the theoretical calculation for Eq. (6) can provide only the cumulants. The two-magnon line shape based on the quantum fluctuation effect is highly desirable to understand the broad B_{1g} spectrum in the 2D antiferromagnet.

A third alternative is that four-magnon scattering is dominant at energies near $4J$. In the case of $\text{La}_2\text{CuO}_{4-y}$, Sugai *et al.*³⁷ found a new spin-excitation peak at $4J$ besides the two-magnon spectrum. They interpret the $4J$ peak in terms of the four-spin cyclic exchange interaction.^{38,39} Simple calculations based on Eq. (1) show that the lowest energies to flip a cluster of two-, four-, and six-spins are $3J$, $4J$, and $5J$, respectively, in the spin- $\frac{1}{2}$, 2D square lattice. However, broad two-magnon features in $L_2\text{CuO}_{4-y}$ prevent us from identifying the four-magnon scattering. Figure 3 shows that near 3800 cm^{-1} ($3.9J$) the deviation from symmetry in the B_{1g} spectrum has a peak whose intensity is about 20% of the two-magnon peak. In the 3D antiferromagnets NiO and KNiF_3 (Ref. 40), a clear distinction has been reported between the two- and four-magnon spectra, presumably because the product Sz is large. The ratio of four- to two-magnon peak-intensities, I_{4M}/I_{2M} , is about $\frac{1}{150}$ in KNiF_3 (Ref. 40). Such a small I_{4M}/I_{2M} for KNiF_3 appears to contradict the assumption that the four-magnon scattering in $\text{Pr}_2\text{CuO}_{4-y}$ occupies 20% of the B_{1g} intensity near $3.9J$.

The observed A_{1g} spectrum in $\text{Pr}_2\text{CuO}_{4-y}$ may contain the predicted broad featureless part at low energies, but the observed A_{1g} spectra for $\text{Nd}_2\text{CuO}_{4-y}$ and $\text{Sm}_2\text{CuO}_{4-y}$ appear to be unfavorable with respect to the predictions. Each A_{1g} spectrum exhibits a peak whose energy corresponds to $\hbar\omega_p$ in the B_{1g} mode. The spin-wave theory fails to predict that the A_{1g} spectrum should have a broad peak whose tail extends to energies higher than $4J$. Having the same $\hbar\omega_p$ values suggests that the A_{1g} spectrum over a wide energy range is also caused by magnetic excitations. The quantum fluctuation theory^{6,11} can account for the broad A_{1g} spectrum characterized by the center of gravity $\hbar\omega_c = 3.6J$.

B. Doped crystals up to $x = 0.13$

Here we discuss the Ce doping effect on two-magnon features in conjunction with the results for hole doping in $\text{La}_{2-x}\text{Sr}_x\text{CuO}_{4-y}$ and $\text{YBa}_2\text{Cu}_3\text{O}_{6+x}$. The exchange constant J derived from the two-magnon peak position is found to be constant in the range $0 < x < 0.13$. Based on the T_N versus x phase diagram,¹⁵ the Néel temperature T_N in $L_{2-x}\text{Ce}_x\text{CuO}_{4-y}$ decreases with increasing x and the partition between AF and SC states exists at $x = 0.14$ up to 20 K. The neutron diffraction results²¹ show that the T_N values for $\text{Pr}_{2-x}\text{Ce}_x\text{CuO}_{4-y}$ are 170 K for

$x = 0.8$ and 120 K for $x = 0.125$. The room-temperature Raman experiments establish that the damped two-magnon scattering in $L_{2-x}\text{Ce}_x\text{CuO}_{4-y}$ exists at temperatures considerably higher than T_N . Consequently, the destruction of long-range order between the planes has little influence on the short-range order interaction between the nearest-neighbor Cu ions. The fact that J is insensitive to T_N means that a small interplanar-exchange-constant J' plays an essential role in the long-range order of $L_{2-x}\text{Ce}_x\text{CuO}_{4-y}$. Thurston *et al.*²¹ showed that the J'/J ratio in $\text{Nd}_2\text{CuO}_{4-y}$ is 3.6×10^{-6} . The existence of spin-pair excitations above T_N can be attributed to the fact that the intraplanar spin-spin correlation length ξ is very large even above T_N .

Superexchange coupling between the two Cu ions is mediated via the intervening O ions. Thus two-magnon features may be explained in terms of the surrounding ion state. The Ce doping in $L_{2-x}\text{CuO}_{4-y}$ introduces electrons at Cu sites, because O $2p$ orbitals are occupied. In a localized picture, electron doping converts some part of the Cu^{2+} ions to Cu^+ ions whose population is proportional to x . The Cu^+ ions have a nonmagnetic $3d^{10}$ or a magnetic $3d^9 4s^1$ configuration. In the $3d^{10}$ case, the average number $\langle z \rangle$ of nearest-neighbor magnetic sites is reduced by substituting Cu^+ ions for Cu^{2+} ions. If $\langle z \rangle$ is decreased by this mechanism, the Green's function predicts that the two-magnon peak for the doped crystal would shift slightly to lower energy. A linear decrease in $\hbar\omega_p$ with substituted nonmagnetic atoms has been observed in the 3D $\text{KNi}_{1-x}\text{Mg}_x\text{F}_3$ system.⁴¹ This behavior indicates that exchange coupling is absent between the Ni^{2+} and Mg^{2+} ions. In view of the $\text{KNi}_{1-x}\text{Mg}_x\text{F}_3$ case, the B_{1g} results for $L_{2-x}\text{Ce}_x\text{CuO}_{4-y}$ are inconsistent with the localized picture that the nonmagnetic Cu^+ ions are randomly mixed with the $S = \frac{1}{2}$ Cu^{2+} ions. There are three possible explanations for the two-magnon behavior. (1) Clusters of Cu^{2+} or Cu^+ ions exist in the doped crystal. In this situation, the creation of Cu^+ ions by Ce doping is expected to have little effect on the local environment of Cu^{2+} ions whose spins are coupled by the extremely large J . (2) The electrons located at Cu^+ ions shift slightly to the surrounding Cu^{2+} ions. We cannot exclude the itinerant picture that the electrons donated by Ce doping are distributed equally to all the Cu sites. (3) If electrons donated by Ce doping produce the $\text{Cu}4s$ state, $\text{Cu}4s$ spins would then polarize by the s - d interaction to screen partially the $\text{Cu}3d$ spin. The effect of $\text{Cu}4s$ electrons on the two-magnon feature may be small, compared with the $\text{Cu}3d^{10}$ situation. In the three cases, the Ce concentration may not be proportional to the decrease in average number $\langle z \rangle$ of nearest-neighbor magnetic sites. This interpretation is based on the fact that J is independent of the Ce concentration.

There are sharp differences in the doping effect on magnon dispersion between electron- and hole-doped systems. In view of Eq. (2), the present results indicate that there is no magnon softening near the zone boundary in $L_{2-x}\text{Ce}_x\text{CuO}_{4-y}$ over the range $0 < x < 0.13$. In $\text{La}_{2-x}\text{Sr}_x\text{CuO}_{4-y}$ (Ref. 4) and $\text{YBa}_2\text{Cu}_3\text{O}_{6+x}$ (Ref. 2), depressed two-magnon peaks move to lower energy with

increasing hole concentration, indicating magnon softening by hole doping.

In $\text{La}_{2-x}\text{Sr}_x\text{CuO}_{4-y}$, holes added by Sr doping participate in O $2p$ orbitals in the CuO_2 planes, and copper remains in the Cu^{2+} state in the range up to $x=0.3$. Holes at O^- ions acquire spin σ which couples with the nearest-neighbor Cu^{2+} spins S_1 and S_2 . Aharony *et al.*⁴² proposed the concept that the introduction of holes at oxygen sites frustrates the AF spin- $\frac{1}{2}$ system. The exchange J_σ between O^- and Cu^{2+} is much larger than the unaffected superexchange J between Cu-Cu ions, because both exchanges are related to the transfer integral t_0 . In this situation, the Hamiltonian $H = J_\sigma \sigma \cdot (S_1 + S_2)$ predicts that the Cu spins connected with O^- become parallel to each other. The frustration caused by Sr doping decreases the J value between Cu-Cu ions and the average number $\langle z \rangle$ of nearest-neighbor magnetic sites. Consequently, the introduction of charges at Cu^{2+} or O^- sites distinguishes the concentration dependence of two-magnon features.

The Ce doping broadens the B_{1g} line shape significantly in $L_{2-x}\text{Ce}_x\text{CuO}_{4-y}$, as shown in Figs. 6(a) and 7(a). The broadening is ascribed to significant magnon damping near the zone boundary. The magnon-damping behavior in the Raman spectra is consistent with the zone-center results observed by neutron scattering in $\text{La}_{2-x}\text{Sr}_x\text{CuO}_{4-y}$ (Refs. 22–25) and $\text{YBa}_2\text{Cu}_3\text{O}_{6+x}$ (Refs. 26–28). Presumably the presence of nonmagnetic Cu^+ ions or frustration due to hole doping gives rise to the magnon damping. In addition, low-energy magnons may couple with the mobile carriers. Thus the strong magnon damping occurs near the zone center corresponding to the long-wavelength limit.

With increasing Ce concentration, an extremely broad B_{2g} peak appears near $\hbar\omega_p$, while the A_{1g} peak at $\hbar\omega_p$ disappears. The observed behavior may be attributed to the change in magnetic symmetry due to the introduction of electrons. In the localized picture, the configuration (y', x') in the ordered $x=0.5$ crystal corresponds to (y, x) in the undoped crystal. Note in Figs. 6(b) and 7(b) that in the heavily doped crystals broad B_{2g} peaks, which are forbidden in D_{2h} symmetry, are comparable to B_{1g} peaks. The fact that both (y', x') and (y, x) yield similar spectra in doped crystals supports the change in magnetic symmetry. In lightly doped crystals, the A_{1g} spectra have broad, diffuse peaks, while in heavily doped crystals, the A_{1g} intensity decreases with increasing energy. Since the doped spin system requires an additional term in Eq.(1), the A_{1g} spectra in doped crystals are expected to become Raman active. Featureless A_{1g} spectra in doped crystals may correspond to the calculated curve presented in Fig. 3.

C. Superconducting and metallic crystals

In the SC and the metallic phases both B_{1g} and B_{2g} spectra exhibit extremely broad peaks whose positions are nearly equal to $\hbar\omega_p$ in the AF phase. The extremely broad peaks in both B_{1g} and B_{2g} modes strongly suggest that the short-range spin fluctuations between Cu atoms persist in electron-doped superconductors. In addition, the heavily damped magnetic excitations in this region

may be characterized by the concentration-independent J value. In contrast, small, energy-independent Raman scattering is found over a large energy range for superconducting $\text{La}_{2-x}\text{Sr}_x\text{CuO}_{4-y}$ (Ref. 4) and $\text{YBa}_2\text{Cu}_3\text{O}_{6+x}$ (Ref. 2). The energy-independent response also originates from spin fluctuations, in view of neutron diffraction.^{22–28} Therefore, the distinctive Raman features in electron- and hole-doped superconductors suggests that the spin-spin correlation length ξ in $L_{2-x}\text{Ce}_x\text{CuO}_{4-y}$ is larger than that for $\text{La}_{2-x}\text{Sr}_x\text{CuO}_{4-y}$ at the same x value. This is consistent with neutron results.^{21,23} As shown in Figs. 6 and 7, the magnetic excitations make no distinction between the SC and the metallic region. This means that the correlation length ξ decreases slowly with increasing Ce concentration x . This interpretation is compatible with the ξ versus x relation observed for $\text{La}_{2-x}\text{Sr}_x\text{CuO}_{4-y}$ (Ref. 23).

V. CONCLUSION

We carried out Raman scattering experiments up to 8000 cm^{-1} at room temperature in order to investigate magnetic excitations in $L_{2-x}\text{Ce}_x\text{CuO}_{4-y}$ ($L = \text{Pr}, \text{Nd},$ and Sm) as a function of Ce concentration. The intrinsic broad B_{1g} line shape in the undoped crystals is attributable to quantum fluctuations. The introduction of electrons by Ce doping significantly broadens the two-magnon peak in the B_{1g} mode, indicating that zone-boundary magnons become damped with increasing Ce concentration. The energy $\hbar\omega_p$ of the two-magnon peak-position in $\text{Pr}_{2-x}\text{Ce}_x\text{CuO}_{4-y}$ is not affected by doping up to $x=0.2$. Similar behavior is found for $\text{Sm}_{2-x}\text{Ce}_x\text{CuO}_{4-y}$ up to 0.17. Therefore, the destruction of long-range order between the planes has little influence on the short-range order interaction between the nearest-neighbor Cu ions. The lack of softening of short-wavelength magnons in these systems is in marked contrast to the softening behavior in $\text{La}_{2-x}\text{Sr}_x\text{CuO}_{4-y}$. With increasing Ce concentration, an extremely broad B_{2g} peak appears near $\hbar\omega_p$, while the A_{1g} peak at $\hbar\omega_p$ disappears. This phenomenon suggests that the introduction of localized electrons changes the magnetic symmetry. In the SC phase of $L_{2-x}\text{Ce}_x\text{CuO}_{4-y}$, both B_{1g} and B_{2g} spectra exhibit extremely broad peaks. This strongly suggests that the short-range spin fluctuations between Cu atoms persist in electron-doped superconductors. The magnetic excitations make no distinction between the SC and the metallic region. The present results combined with the neutron diffraction results imply that the correlation length ξ decreases slowly with increasing Ce concentration x . Comparison with the Raman results for $\text{La}_{2-x}\text{Sr}_x\text{CuO}_{4-y}$ suggests that the correlation length in the electron-doped superconductors is considerably larger than that for the hole-doped superconductors.

ACKNOWLEDGMENTS

We are grateful to J. O. Willis for valuable discussions. A part of this work was supported by the New Energy and Industrial Technology Development Organization under the management of the R&D of Basic Technology for Future Industries.

- ¹K. B. Lyons, P. A. Fleury, J. P. Remeika, A. S. Cooper, and T. J. Negran, *Phys. Rev. B* **37**, 2353 (1988).
- ²K. B. Lyons, P. A. Fleury, L. F. Schneemeyer, and J. V. Waszczak, *Phys. Rev. Lett.* **60**, 732 (1988).
- ³K. B. Lyons and P. A. Fleury, *J. Appl. Phys.* **64**, 6075 (1988).
- ⁴S. Sugai, S. Shimoto, and M. Sato, *Phys. Rev. B* **38**, 6436 (1988).
- ⁵K. B. Lyons, P. E. Sulewski, P. A. Fleury, H. L. Carter, A. S. Cooper, G. P. Espinosa, Z. Fisk, and S.-W. Cheong, *Phys. Rev. B* **39**, 9693 (1989).
- ⁶R. P. Singh, P. A. Fleury, K. B. Lyons, and P. E. Sulewski, *Phys. Rev. Lett.* **62**, 2736 (1989).
- ⁷T. Tokura, H. Takagi, and S. Uchida, *Nature (London)* **337**, 345 (1989).
- ⁸H. Takagi, S. Uchida, and Y. Tokura, *Phys. Rev. Lett.* **62**, 1197 (1989).
- ⁹J. T. Markert, E. A. Early, T. Bjornholm, S. Ghamaty, B. W. Lee, J. J. Neumeier, R. D. Price, C. L. Seaman, and M. B. Maple, *Physica C* **158**, 178 (1989).
- ¹⁰S. Sugai, T. Kobayashi, and J. Akimitsu, *Phys. Rev. B* **40**, 2686 (1989).
- ¹¹P. E. Sulewski, P. A. Fleury, K. B. Lyons, S.-W. Cheong, and Z. Fisk, *Phys. Rev. B* **41**, 225 (1990).
- ¹²J. Akimitsu, H. Sawa, T. Kobayashi, H. Fujiki, and Y. Yamada, *J. Phys. Soc. Jpn.* **58**, 2646 (1989).
- ¹³Y. Endo, M. Matsuda, K. Yamada, K. Kakurai, Y. Hidaka, G. Shirane, and R. J. Birgeneau, *Phys. Rev. B* **40**, 7023 (1989).
- ¹⁴D. E. Cox, A. I Goldman, M. A. Subramanian, J. Gopalakrishnan, and A. W. Sleight, *Phys. Rev. B* **40**, 6998 (1989).
- ¹⁵S. Uchida, H. Takagi, Y. Tokura, N. Koshihara, and T. Arima, in *Strong Correlation and Superconductivity*, edited By H. Fukuyama, S. Maekawa and A. P. Malozemoff (Springer, Berlin/Heidelberg, 1989).
- ¹⁶G. M. Luke, B. J. Sternlieb, Y. J. Uemura, J. H. Brewer, R. Kadono, R. F. Kiefl, S. R. Krietzman, T. M. Riseman, J. Gopalakrishnan, A. W. Sleight, M. A. Subramanian, S. Uchida, H. Takagi, and Y. Tokura, *Nature (London)*, **338**, 49 (1989).
- ¹⁷K. Oka and H. Unoki, *Jpn. J. Appl. Phys.* **28**, L937 (1989).
- ¹⁸K. Oka and H. Unoki, *Jpn. J. Appl. Phys.* **29**, L909 (1990).
- ¹⁹J. B. Parkinson, *J. Phys. C* **2**, 2012 (1969).
- ²⁰R. J. Elliott and M. F. Thorpe, *J. Phys. C* **2**, 1630 (1969).
- ²¹T. R. Thurston, M. Matsuda, K. Kakurai, K. Yamada, Y. Endoh, R. J. Birgeneau, P. M. Gehring, Y. Hidaka, M. A. Kastner, T. Murakami, and G. Shirane, *Phys. Rev. Lett.* **65**, 263 (1990).
- ²²G. Aeppli, S. M. Hayden, H. A. Mook, Z. Fisk, S.-W. Cheong, D. Rytz, J. P. Remeika, G. P. Espinosa and A. S. Cooper, *Phys. Rev. Lett.* **62**, 2052 (1989).
- ²³R. J. Birgeneau, D. R. Gabbie, H. P. Jenssen, M. A. Kastner, P. J. Picone, T. R. Thurston, G. Shirane, Y. Endoh, M. Sato, K. Yamada, Y. Hidaka, M. Oda, Y. Enomoto, M. Suzuki, and T. Murakami, *Phys. Rev. B* **38**, 6614 (1988).
- ²⁴K. Yamada, K. Kakurai, Y. Endoh, T. R. Thurston, M. A. Kastner, R. J. Birgeneau, G. Shirane, Y. Hidaka, and T. Murakami, *Phys. Rev. B* **40**, 4557 (1989).
- ²⁵T. R. Thurston, R. J. Birgeneau, M. A. Kastner, N. W. Preyer, G. Shirane, Y. Fujii, K. Yamada, Y. Endoh, K. Kakurai, M. Matsuda, Y. Hidaka, and T. Murakami, *Phys. Rev. B* **40**, 4585 (1989).
- ²⁶J. M. Tranquada, W. J. Buyers, H. Chou, T. E. Mason, M. Sato, S. Shimoto, and G. Shirane, *Phys. Rev. Lett.* **64**, 800 (1990).
- ²⁷J. M. Tranquada, G. Shirane, B. Keimer, S. Shimoto, and M. Sato, *Phys. Rev. B* **40**, 4503 (1989).
- ²⁸G. Shirane, J. Nielsen, M. Nielsen, J. M. Tranquada, H. Chou, S. Shimoto, and M. Sato, *Phys. Rev. B* **41**, 6547 (1990).
- ²⁹F. C. Zhang and T. M. Rice, *Phys. Rev. B* **37**, 3759 (1988).
- ³⁰W. H. Weber and G. H. Ford, *Phys. Rev. B* **40**, 6890 (1989).
- ³¹P. A. Fleury and H. J. Guggenheim, *Phys. Rev. Lett.* **24**, 1346 (1970).
- ³²S. L. Cooper, G. A. Thomas, J. Orenstein, D. H. Rapkin, A. J. Millis, S.-W. Cheong, A. S. Cooper, and Z. Fisk, *Phys. Rev. B* **41**, 11605 (1990).
- ³³Y. Tokura, N. Koshihara, T. Arima, H. Takagi, S. Ishibashi, T. Ido, and S. Uchida, *Phys. Rev. B* **41**, 11657 (1990).
- ³⁴S. Chakravarty, B. I. Halperin, and D. R. Nelson, *Phys. Rev. B* **39**, 2344 (1989).
- ³⁵J. F. Annett, R. M. Martin, A. K. McMahan, and S. Satpathy, *Phys. Rev. B* **40**, 2620 (1989).
- ³⁶E. Dagotto and A. Moreo, *Phys. Rev. Lett.* **63**, 2148 (1989).
- ³⁷S. Sugai, M. Sato, T. Kobayashi, J. Akimitsu, T. Ito, H. Takagi, S. Uchida, S. Hosoya, T. Kajitani, and T. Fukuda, *Phys. Rev. B* **42**, 1045 (1990).
- ³⁸M. Roger and J. M. Delrieu, *Synth. Met.* **29**, F673 (1989).
- ³⁹H. J. Schmidt and Y. Kuramoto, *Physica B* **163**, 443 (1990).
- ⁴⁰R. E. Dietz, W. F. Brinkman, A. E. Meixner, and H. J. Guggenheim, *Phys. Rev. Lett.* **27**, 814 (1971).
- ⁴¹P. A. Fleury, W. Hayes, and H. J. Guggenheim, *J. Phys. C* **8**, 2183 (1975).
- ⁴²A. Aharony, B. J. Birgeneau, A. Coniglio, M. A. Kastner, and E. H. Stanley, *Phys. Rev. Lett.* **60**, 1330 (1988).